Lateral Leakage in Silicon Photonics: Theory, Applications, and Future Directions

Thach G. Nguyen, *Member, IEEE*, Andreas Boes, *Member, IEEE*, and Arnan Mitchell, *Senior Member, IEEE*

(Invited Paper)

***Abstract*—This paper presents an overview of lateral leakage in silicon photonics due to polarization coupling between the guided mode of a ridge waveguide and unguided slab mode in the etched cladding. We explain the physical origins and provide insight into how this effect can be suppressed or harnessed. We show how lateral leakage can manifest as new resonant behaviour and explore this effect in the context of bound states in the continuum. We review a number of applications for devices based on lateral leakage and present outlook for a new generation of polarization manipulators, antennas and filters.**

***Index Terms*—Silicon photonics, optical waveguide, optical resonator, bound states in the continuum.**

I. Introduction

SILICON photonics has been commonly accepted as the key technology for low cost, mass manufacturable and high density photonic integrated circuits (PICs). Commercial applications of silicon photonics are now widely available in data communications and sensing.

Low loss optical waveguides are the fundamental component of PICs. Photonic waveguides in silcon-on-insulator (SOI) wafers are formed by either fully etching the silicon layer (wire waveguides) or partially etching the silicon layer (ridge waveguides). Wire waveguides typically have stronger field confinement hence can have lower bending radius than ridge waveguides. On the other hand, ridge waveguides are preferable for some device structures such as modulators and can have lower loss than wire waveguide due to lower etching depth and hence reduced exposure to sidewall roughness. It is commonly believed that high index contrast SOI ridge waveguides do not support the TM polarized mode due to strong lateral leakage [1], [2].

Lateral leakage is an often overlooked effect that can occur in a waveguide that is made in high index contrast film (e.g. silicon) using a shallowly etched ridge. In such a configuration it is possible for the guided mode in the ridge to couple to nominally orthogonally polarized slab modes that have higher effective refractive indices in the slabs outside the ridge. The coupling from the waveguide mode to the slab modes is usually an unwanted parasitic process that contributes to the waveguide loss. In PICs, the lateral leakage effect was first observed in 2007 in the Silicon-On-Insulator (SOI) platform [3]. There it was observed that the TM waveguide modes exhibited unexpectedly high losses, which could be explained by the unintentional coupling to radiation TE slab modes. Interestingly, it was also observed that for some specific waveguide geometries shallowly etched SOI waveguides could also support very low loss TM mode propagation. This was attributed to the resonant cancellation of lateral leakage, an effect that was predicted and observed earlier in rib waveguides at millimeter-wave frequency [4], [5].

There has been a number of reports from researchers aiming to understand and overcome this lateral leakage and leakage cancellation in single straight SOI ridge waveguides as well more sophisticated waveguide configurations as couplers, rings, disks and other waveguide platforms [6]–[13]. On the other hand, rather than viewing lateral leakage as an undesirable loss mechanism, it can be considered as a means of generating controlled coherent beams of TE light that can be engineered for new photonic functions.

Recently, there has been an increased interest in realizing the so-called bound states in the continuum (BICs) using photonic structures, which was first proposed by von Neumann and Wigner in 1929 [14]. BICs are special states of discrete guided waveforms that lie within a continuous spectrum of radiating waves but still remain localized without coupling to the continuum of radiation. This effect can be achieved by symmetry-protected bound states or radiation cancellation through parameter tuning. Structures with BICs can be used to realize high-Q resonators for various applications such as filtering, sensing and lasing [14]. In light of the BIC theory, one can see that the lateral leakage and leakage cancellation are in fact BICs.

We believe that the majority of researchers in the PIC community are unaware of the lateral leakage effect, how and when it will occur and its potential applications in polarization filtering and long range transport among others. In this contribution, we would like to introduce this effect to the wider PIC community and give a brief overview of the lateral leakage effect. We also show that the reverse process is possible, where an unbound beam of light is used to excite the guided mode of a ridge and

Manuscript received June 3, 2019; revised July 26, 2019; accepted August 6, 2019. Date of publication August 19, 2019; date of current version August 30, 2019. This work was supported by the Australian Research Council Discovery Projects Program under Grant DP150101336. *(Corresponding author: Thach G. Nguyen.)*

The authors are with the School of Engineering, RMIT University, Melbourne, VIC 3000, Australia (e-mail: thach.nguyen@rmit.edu.au; andreas.boes@rmit.edu.au; arnan.mitchell@rmit.edu.au).

Color versions of one or more of the figures in this article are available online at http://ieeexplore.ieee.org.

Digital Object Identifier 10.1109/JSTQE.2019.2935315

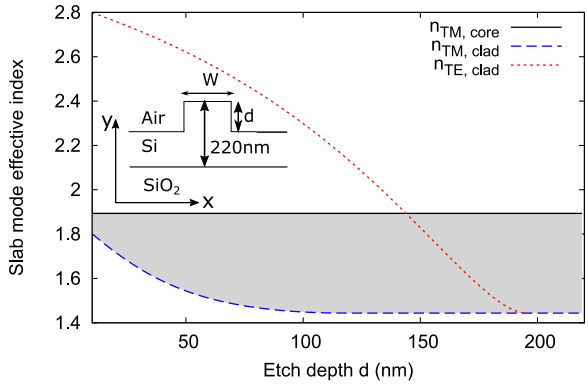

Fig. 1. Effective indices of TE/TM slab modes in the core and cladding regions of a SOI ridge waveguide as a function of etch depth h. Waveguide cross-section is illustrated in the inset.

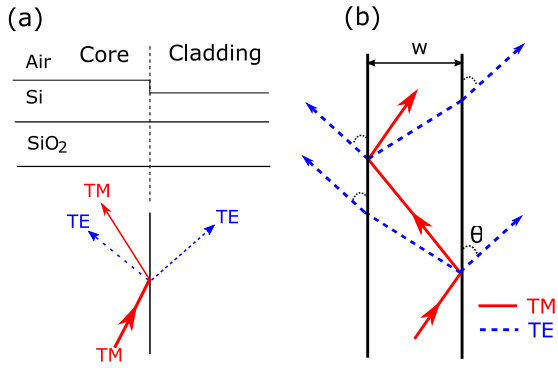

Fig. 2. Mode coupling diagram showing the TM-TE mode coupling at the ridge boundary: (a) when TM slab mode is obliquely incident on the boundary; and (b) lateral leakage due to interference of TE waves from both boundaries.

that this holds great promise for a new generation of integrated wavelength filters and as a platform for exploration of the physics of BICs and other related physical phenomena.

II. Lateral Leakage Background

This Section describes the background of the lateral leakage effect and is structured as follows: Section II-A describes the origin of the lateral leakage effect; Section II-B details the circumstances under which this leakage can be cancelled; Section II-C specifies how lateral leakage can be effectively simulated; Section II-D outlines the experimental observation of lateral leakage in SOI platform; Section II-D gives examples of lateral leakage in other platforms than silicon; Section II-F describes the behaviour of lateral leakage in curved structures such as disks and rings and finally Section II-G gives an overview of coupled waveguides exhibiting lateral leakage. This background will form a basis for our exploration of applications of lateral leakage and the relationship to bound states in the continuum.

A. Origin of Lateral Leakage

In this Section, we give a brief overview of the physical origin of the lateral leakage effect, based on thin-ridge waveguides in the SOI platform. Fig. 1 presents the effective index of the TE and TM modes of a 220 nm thick slab of silicon as a function of etch depth. The effective indices of the TM mode for the un-etched slab are also presented for reference. It can be seen that the fundamental TE mode of the etched slab remains higher than the fundamental TM mode of the unetched slab until the etch depth approaches 150 nm. This rather surprising result can be attributed to the relatively thin silicon film and the strong index contrast between the silicon core and silica/air cladding materials. The boundary conditions for the TM mode at the high index contrast interfaces results in a far stronger evanescent field for the TM mode outside of the core material when compared to the TE mode. The inset of Fig. 1 illustrates a typical ridge waveguide cross-section. It is easy to see that for etch depths less than 150 nm, the fundamental TM mode guided by the ridge could be phase matched to unguided TE radiation in the slab.

One might expect that the TM waveguide mode and TE slab mode should not couple to each other as they are nominally orthogonal. However, the guided TM mode has a strong longitudinal electric field component E_z, which is a consequence of the high index contrast. Similarly, the unguided TE radiation can propagate at any angle relative to the waveguide axis. As the direction of propagation is rotated away from the waveguide axis, the electric field which is transverse to the direction of propagation will be rotated onto the waveguide axis, resulting in a relatively strong field component E_z. As a result, the mode field overlap between the guided TM mode and the TE slab mode propagating at an angle can be non-zero, particularly when purturbed by the etched ridge which breaks vertical symmetry. Furthermore, the guided TM mode and the radiating TE slab mode can be phase-matched, depending on the propagation angle of the slab mode. Therefore, these two modes can couple quite strongly. The index discontinuity at the ridge walls acts as a perturbation to cause mode conversion, resulting in lateral leakage of the guided TM mode into the radiating TE slab mode.

It has been shown that there is significant TM-TE mode coupling at the ridge boundaries, when the fundamental TM mode of the ridge core region is obliquely incident on the ridge interface from the ridge core [15]. Under total internal reflection, a small amount of power is coupled into a transmitted TE slab mode propagating in the cladding region and a small amount of power is reflected and propagates as a reflected TE slab mode in the core region as illustrated in Fig. 2(a). The transmitted and reflected TE slab modes have similar but not identical magnitude and a small phase difference [15].

Due to the TM/TE mode conversion at the ridge walls, the guided TM mode progressively loses power to the TE slab modes radiating outside the waveguide core region as illustrated in Fig. 2(b). This loss of power from the guided TM mode to the unguided TE mode is called lateral leakage. It should also be noted that this loss is quite different to scattering loss or absorption as it results in highly coherent TE radiation which is confined vertically but radiates at a precise angle θ to the waveguide axis given by:

$$\theta = \cos^{-1}\left(\frac{N_{TM}}{n_{TE}^{clad}}\right) \tag{1}$$

where N_{TM} is the effective index of the guided TM mode, n_{TE}^{clad} is the effective index of fundamental TE slab mode of the cladding region outside the waveguide core.

B. Leakage Cancellation

When a guided TM mode propagates in the ridge, it continues to lose power to the TE slab modes radiating on both sides of the ridge. The intensity of the radiating TE wave is the coherent sum of the transmitted and reflected TE waves generated at both ridge walls. Therefore, the intensity of the lateral leakage depends on the phase difference between transmitted and reflected TE waves generated at the two ridge walls. This phase difference is a function of the ridge width. For some particular widths, these two beams of TE radiation can interfere destructively, resulting in the resonant cancellation of lateral leakage. In this case the ridge waveguide will experience the lowest loss from the lateral leakage effect, when operated in transmission and excited with the TM waveguide mode. The resonant widths W can be readily predicted as [3], [15]:

$$W = \frac{(m + \Delta\phi/(2\pi))\,\lambda}{\sqrt{(n_{TE}^{core})^2 - N_{TM}^2}} \tag{2}$$

where m is a non-zero integer, $\Delta\phi$ is the phase difference between the reflected and transmitted TE waves and λ is the wavelength. The resonant widths at which the resonant cancellation of the lateral leakage takes place have been termed 'magic' widths [15].

C. Simulation of Lateral Leakage

The lateral leakage loss of the guided TM mode can be calculated from the imaginary part of the mode effective index. To calculate the effective index of the ridge waveguide mode, an eigenmode solver with transparent boundaries in the lateral direction must be used in order to correctly simulate the lateral leakage behaviour due to the strong lateral radiation. It is technically possible to simulate waveguides with lateral leakage using a traditional finite element or finite difference solver with perfectly matched layer boundaries; however great care must be taken to optimize the absorbing boundary condition properties [15]. As an alternative, we have found that the semi-analytical mode-matching method [5], [16] is very suitable for this task since the computational window is fully open in the lateral direction.

As an example, we used a mode solver based on the semi-analytical mode-matching method to simulate the effective index and leakage loss of the TM mode as a function of ridge core width for different etch depths. The results of the simulation can be seen in Fig. 3. It can be seen in Fig. 3(a) that the TE slab mode has a higher effective refractive index than the TM waveguide mode for etch depths of 30, 70 and 110 nm, independent of the ridge core width. For an etch depth of 150 nm, the effective refractive index of the TM waveguide mode is higher than the TE slab mode for a ridge core width above 1010 nm. These findings match well with the results in Fig. 1, where we found that when the etch depth is below 150 nm, the effective index of the guided

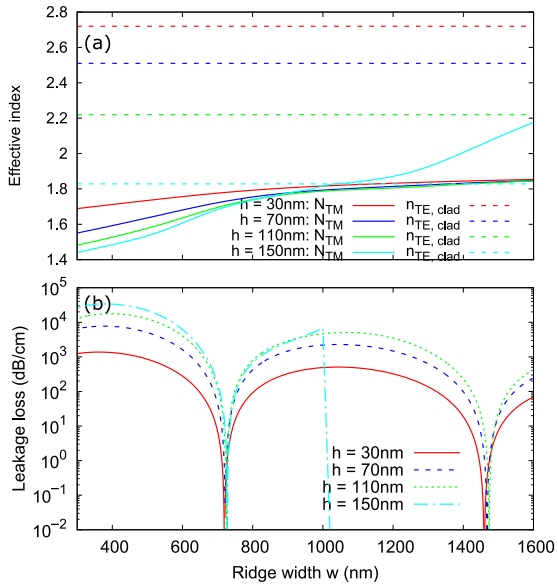

Fig. 3. Simulated mode effective index (a) and leakage loss (b) as a function of ridge width for different etch depth.

TM mode is always lower than that of the TE slab mode in the cladding regions regardless the ridge width. Therefore, the guided TM mode can always exhibit leakage behaviour when etch depth is less than 150 nm. However, when the etch depth is higher than 150 nm, the effective index of the guided TM mode can be higher than that of the TE slab mode in the cladding. In these cases, lateral leakage cannot occur.

In Fig. 3(b), one can see that the leakage loss is strongly dependent on the ridge core width with periodic features. One can further see that for a ridge core width of 722 nm and 1415 nm the leakage loss can be very low. These ridge core widths are the 'magic' widths where leakage loss is cancelled, as described in Section II-B. The simulated 'magic' widths are in excellent agreement with values calculated using Eq. 2. The 'magic' widths only vary slightly for different etch depths. This is due to weak dependence of the effective index of the guided TM mode on the etch depth as shown in Fig. 3(a).

It should be noted that leakage cancellation at the 'magic' widths is not perfect since the transmitted and reflected TE waves generated at each ridge boundary are not identical in magnitude [15]. However, at these widths, the leakage loss is still much lower than other loss mechanisms such as scattering loss due to surface roughness [3].

One can further see in Fig. 3(b) that for an etch depth of 150 nm the leakage loss suddenly drops sharply at the ridge core width of 1010 nm. At this point the effective refractive index of the TM waveguide mode becomes larger than the TE slab modes, hence lateral leakage loss ceases to occur.

Furthermore, it can be observed that for a given ridge width, the leakage loss increases with increasing etch depth. This can be explained due to the larger perturbation region at the ridge boundary leading to stronger TM/TE mode conversion.

In Figs. 4(a) and (b) the vectorial field components of the guided TM mode for an etch depth of 70 nm are shown for a

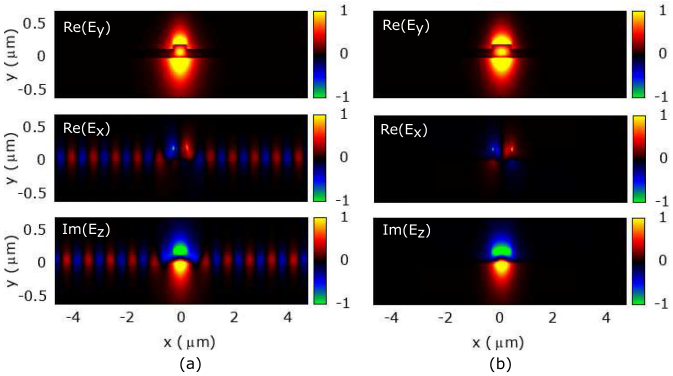

Fig. 4. Electric field distributions of the TM-like mode for (a) 550 nm and (b) 722 nm waveguide widths.

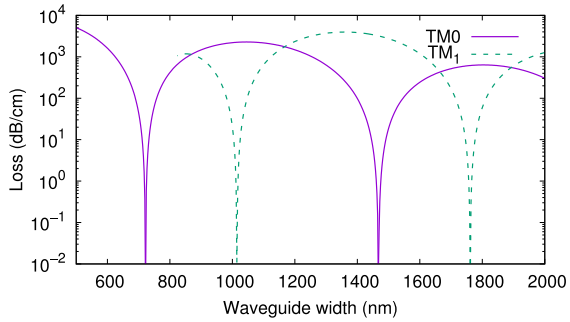

Fig. 5. Simulated leakage loss as a function of ridge width for TM_0 and TM_1 modes. The etch depth is 70 nm.

core width of 550 nm (non-'magic' width) and a core width of 722 nm ('magic' width), respectively. It can be seen that for a core width of 550 nm [Fig. 4(a)] a strong radiating TE field propagating at an angle to both sides of the ridges is evident, indicating a high leakage loss. Whereas, there is no propagating TE field outside the ridge for a core width of 722 nm, confirming the occurrence of leakage cancellation.

When the ridge core width is sufficiently large, the ridge can support more than one guided TM mode. The higher order TM modes can also exhibit lateral leakage as well as 'magic' width behaviour. It can be seen from Eq. 2 that the leakage cancellation widths should be different for different guided TM mode orders because of the difference in mode effective index N_{TM}. Fig. 5 shows the leakage loss for the fundamental TM_0 and first order TM_1. The leakage loss for TM_1 mode is very strong when the leakage loss for TM_0 mode is cancelled. This phenomena allows relatively wide waveguides with effectively single-mode behaviour as even though a first order mode is technically supported, the leakage loss will deplete this mode before any significant transmission occurs.

As discussed in Section II-B, the strength of the lateral leakage depends on the relative phase of the generated TE waves at both ridge boundaries. As the phase is a function of wavelength, it is expected that leakage loss and leakage cancellation also depends on wavelength. To show this, we simulated the leakage loss as a function of wavelength for different ridge widths around the

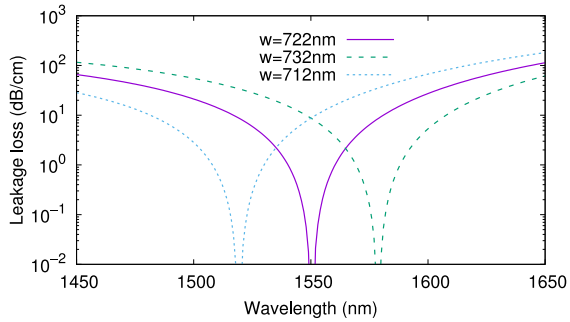

Fig. 6. Leakage loss as a function of wavelength for different ridge widths close to the 'magic' width.

first 'magic' with $W = 722$ nm. The results are shown in Fig. 6, where it can be seen that the 'magic' width wavelength shifts by about 30 nm for a 10 nm change in ridge core width. This wavelength behaviour suggests possible utility in wavelength filtering.

D. Experimental Observation of Lateral Leakage in SOI Ridge Waveguides

The potential for lateral leakage behaviour in strip and rib waveguides was in fact first theoretically predicted by Peng and Oliner in 1978 [1]. They also found that the leakage can be effectively cancelled if the waveguide geometries meet certain criteria. The leakage and leakage cancellation effects were also theoretically analyzed and later experimentally verified on strip waveguides at millimetre-wave frequencies by Ogusu *et al.* [5], [17], [18]. The first experimental observation of the lateral leakage and leakage cancellation behaviours in the optical waveguides were made on shallowly etched thin ridge SOI waveguides using non-standard processing techniques in 2007 [3]. The width dependence of the TM mode propagation loss was also experimentally observed in ridge waveguides fabricated using standard silicon foundry fabrication [19]. The experimental results matched very well with the theoretical prediction. Drastic reduction of the propagation loss were observed at the 'magic' widths of 0.72 μm and 1.44 μm [3], [19], confirming the theoretical predictions. In [19], the existence of strong TE radiation as well as suppression of this radiation at the 'magic' widths were also demonstrated by directly observed the radiating TE field on both sides of the ridge. Further investigations have demonstrated that the lateral leakage loss can be electrically tuned when using liquid crystal (LC) as the cladding materials [20], [21].

E. Lateral Leakage in Non-Ridge SOI Waveguides or Non-Silicon Waveguides

The lateral leakage and leakage cancellation behaviours are not limited to thin-ridge SOI waveguides. These behaviours can also occur in other high index contrast ridge waveguides if the effective indices of the slab modes in the cladding region are higher than the effective index of the guided mode in the core. Similar lateral leakage and leakage cancellation characteristics have been shown for horizontal slot waveguides [22], symmetric

and asymmetric rib-type slot waveguides [6], silicon nitrite ridge waveguides [12], a low refractive index waveguide on a high refractive index thin membrane [13], and even anisotropic lithium niobate on insulator (LNOI) waveguides [8]. Similar phenomena have also been observed in an anti-resonant reflecting optical waveguide (ARROW) and deep, thick ridge waveguides [23] as well as whispering-gallery modes of microcylinder resonators [24], [25]. However, in these cases, the mode coupling occurs in the vertical direction.

Recently, it has been found that similar lateral leakage behaviour can also occur in X-cut thin-film lithium niobate with silicon nitrite ridge loaded waveguides. Here, due to the birefringent of $LiNbO_3$, the roles of the TE and TM polarisations are reversed with the effective index of the TM slab mode in the cladding being higher than that of the TE guided mode in the ridge. This can lead to coupling from TE guided mode to TM slab mode [26].

F. Lateral Leakage in Disks and Rings

In the previous Sections, the theory of lateral leakage and leakage cancellation phenomenon in straight ridge SOI waveguide for TM-like guided mode has been presented. In this Section, the lateral leakage behaviour in ridge SOI waveguides when used in disk and ring resonator configurations is explored.

Similar to a straight waveguide, TM to TE mode conversion can happen at the ridge interface of a shallowly etched SOI disk. This mode conversion generates a TE beam which propagates away from the disk, and a reflected TE beam which traverses a secant across the disk, transmits through the disk boundary and then radiates away from the disk, similar to the first TE beam, but at an advanced azimuthal angle. This TM to TE coupling can cause leakage loss for the TM whispering gallery mode. Similar to the case of straight waveguides, outside the disk, there are two different types of TE beam having similar magnitudes. The phase difference between these two TE beams depends only on the disk radius. Hence, for some particular disk radii, it is possible for these two TE beams to interfere destructively resulting in low leakage loss [27]. Whereas, inside the disk there is only the reflected TE beam generated from the TM-TE conversion at the disk boundary, independent of the disk radius [27].

The lateral leakage behaviour of disks can be rigorously simulated using a full-vectorial mode-matching model based on radial coordinates [28] with fully open simulation window in radial direction. Fig. 7 shows the simulated propagation loss of the first three TM whispering gallery modes as a function of the disk radius. The calculated propagation loss includes both the lateral leakage loss as well as the traditional bending loss. The propagation loss exhibits a cyclic dependence on the disk radius. For some particular disk radii, the disks have low propagation loss due to the cancellation of lateral leakage loss that can be predicted using a simple geometric model [27]. At these radii, the loss is dominated by the traditional bending loss when the disk radius is small. It has been shown that when leakage cancellation occurs, there is no radial (TE) field component of the whispering gallery mode outside the disk as expected. However, there is always broad and strong radial field component

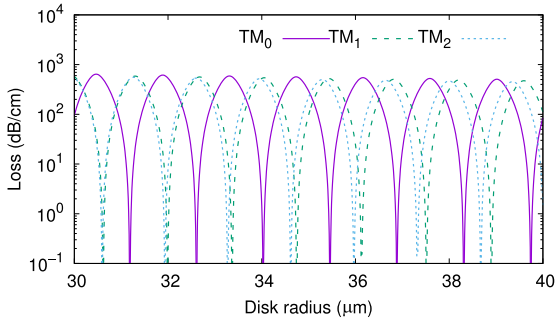

Fig. 7. Loss of the first three TM-like whispering gallery modes of disk resonators as a function of the disk radius.

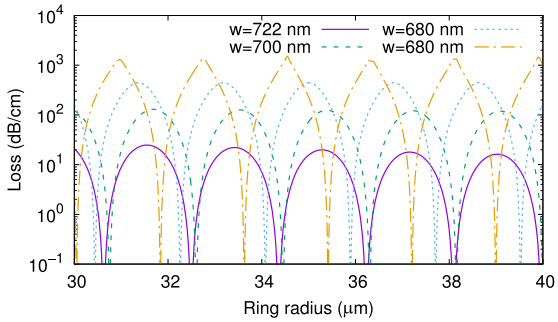

Fig. 8. Loss of the TM mode as a function of the ring radius for different ridge core widths.

inside the disk regardless of the strength of leakage [27]. This is the case since inside the disk there is only reflected TE waves generated at the disk boundary from TM/TE conversion.

When a thin-ridge waveguide is formed into a ring, the reflected TE wave generated on the outer boundary of the ring, and the transmitted TE wave generated on the inner boundary of the ring can traverse across the ring, intersect with the ring waveguide and then propagate outside the ring again. Thus, inside the ring, there are two different TE beams while there are four beams of TE radiation outside the ring. The amplitude of the TE field outside the ring is the coherent superposition of these four beams and this will determine the lateral leakage loss. The relative phases of the TE waves outside the ring depend not only on the waveguide ridge width but also on the ring radius. Therefore, there exists some combination of waveguide width and ring radius so that all TE beams outside the ring interfere destructively resulting in low leakage loss. Inside the ring, the relative phase between TE waves, and hence the amplitude of TE field, is determined only by the waveguide width and so this can be large, even if the leakage outside the ring is cancelled.

Figure 8 shows the calculated propagation loss of the fundamental TM mode as a function of the ring radius for different ridge core widths using a mode-matching model in radial coordinates. Although the loss calculated from the mode-matching model includes both lateral leakage loss and traditional bending loss, the bending loss is negligible for the relatively large radius rings considered. Thus, the losses shown in Fig. 8 are mainly

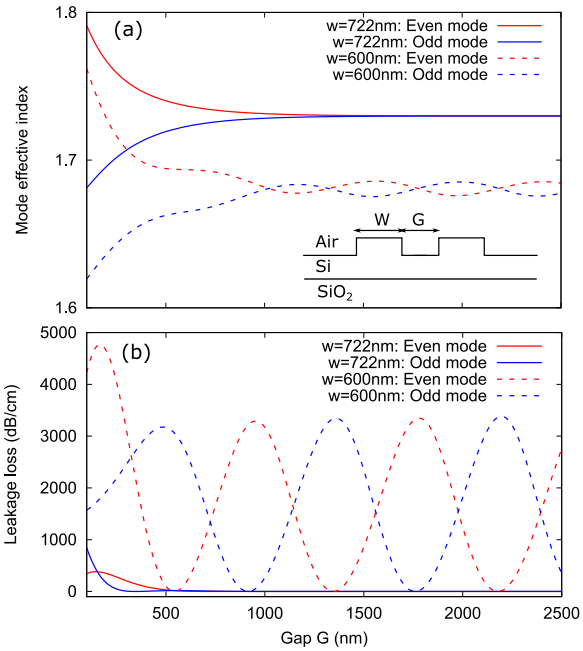

Fig. 9. Leakage loss of even and odd supermodes of two parallel waveguide structure as a function of gap between two waveguides for different ridge widths.

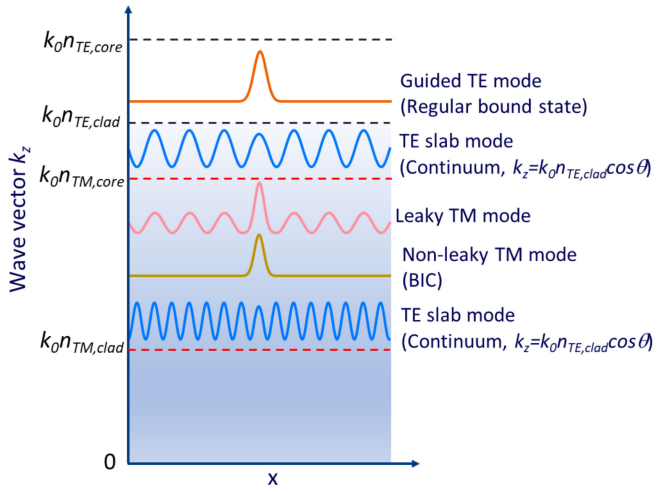

Fig. 10. Illustration of the spectrum of modes and their spatial profiles in a thin-ridge SOI waveguide. The shaded region indicates the continuum of TE slab radiation. The two dashed red lines indicates the region of discrete guided TM modes.

due to lateral leakage. As predicted, the lateral leakage loss shows a strong dependence on both waveguide width and ring radius. Similar to the case of disks, the lateral leakage loss of rings varies periodically with ring radius. For each waveguide width, there exists some ring radii where the leakage loss is effectively cancelled. When the waveguide width is exactly equal the 'magic' width of a straight waveguide, low leakage loss is not always possible except when combing with a specific ring radius. This can be explained by considering the imbalance of the reflected and transmitted TE waves generated from TM-TE mode coupling from the two waveguide boundaries [15]. This small imbalance in a perfectly straight waveguide is exacerbated in a ring due the difference in the radii of the inner and outer waveguide boundaries of the ring.

G. Lateral Leakage in Coupled Waveguides

Many device structures can be formed from coupled waveguides such as directional couplers. When two waveguides are placed next to each other as illustrated in the inset of Fig. 9, the behaviour of the structure can be rigorously represented as a superposition of the even and odd supermodes of the structure. In this Section, we will investigate the leakage behaviour of the supermodes.

It has been shown previously [15] that the lateral leakage loss of the supermodes depends on both the ridge width and spacing between two ridges. Using the mode-matching model, the complex effective indices of the even and odd supermodes were simulated and are shown in Fig. 9 as a function of the gap between two ridges. Two ridge widths were considered, one is the 'magic' width of a single ridge waveguide and one is at the 'non-magic' width. Although when the ridge width is at the 'magic' width of the single ridge waveguide, it is not always possible to achieve low leakage loss on both supermodes unless the two ridges are far apart resulting in weak evanescent coupling.

When the single ridge leaks strongly, the two guided TM modes of the two ridges can still couple via the TE leakage even with large separation between the two ridges where the evanescent coupling is negligible. This coupling oscillates with the gap. Since this coupling is via the radiating TE wave, it does not reduce with increasing the gap. The leakage loss of the odd and even supermodes also oscillates as a function of the gap, but with opposite phase. It is not possible to have both modes with low loss at the same time. When one mode has zero leakage loss, the other mode has maximum loss and vice verse. However, in this case, the two supermodes have identical phase velocity.

III. Lateral Leakage as Bound State in the Continuum

Recently, there has been a great deal of scientific interest in bound states in the continuum (BIC's) in photonic structures [14]. BIC's are special eigenmodes of structures that have open scattering channels. In most cases, the power of the eigenmodes leak into these scattering channels. However, under some special circumstances, the leakage is cancelled, resulting in localized modes within the continuum of scattering channels.

Comparing with BIC behaviour, we can see that the effects of low loss propagation of the TM mode in a thin-ridge SOI waveguide due to leakage cancellation can also be considered as guiding light through optical bound states in the continuum. The TE waves radiated from both sides of the ridge are scattering channels. Fig. 10 illustrates the spectrum and the spatial profile of the modes of a thin-ridge SOI waveguide. The vertical axis in Fig. 10 is the component along the waveguide axis of the wave vector k_z. Shown at the top are the discrete levels of the guided TE modes of the ridge waveguide. These guided TE modes are conventional bound states. Below the discrete guided

TE modes are the continuum of radiating TE slab modes. It is important to note that these TE slab modes form a continuous spectrum, not at discrete levels. Although these TE slab modes are confined vertically, they can propagate at an arbitrary angle θ to the waveguide axis. The component of the wave vector along the waveguide axis is $k_z = k_0 n_{TE,clad} \cos\theta$, where $k_0 = 2\pi/\lambda$ is the free-space propagation constant. Therefore, these TE slab modes form a continuum in the mode spectrum with the wave vector extending from zero to $k_0 n_{TE,clad}$. These TE slab modes are the scattering channels. The discrete guided TE modes have no access to these scattering channels, hence remain uncoupled from these channels. As shown in Fig. 1, the effective index of the un-etched silicon core $n_{TM,core}$ can be lower than $n_{TE,clad}$. Therefore, the guided TM modes can lie inside the continuum of laterally radiating TE slab modes, thus can couple to these scattering channels. BIC's are formed when having destructive interference of various scattering channels under certain conditions of ridge width (for the case of straight waveguides) and/or the radius (for the case of rings/disks), resulting in cancellation of loss to the continuum. Under these conditions, the discrete guided TM modes lie within the continuum of radiating TE slab modes but still remain isolated without coupling to the continuum of radiation. This type of BIC in thin-ridge SOI waveguides can be considered as single-resonance parametric BIC [14]. Similar BIC behaviour has also been predicted to exist in a low refractive index waveguide on a high refractive index thin membrane [13].

In the coupled waveguide structures of Fig. 9, BIC's also exist at some specific gaps between the two ridges where the leakage loss of one supermode is zero. This is a type of Fabry-Perot BIC formed by coupling between two identical resonances [14]. In this BIC, two identical resonances (two leaky TM modes) couple to the same radiation channel (TE slab mode). When the round trip phase shift of the TE radiation is multiple of 2π, the TE wave can be trapped in between the two ridges to form a standing wave while there is no TE radiation outside the ridges [14].

IV. Applications of Lateral Leakage

The lateral leakage behaviour of TM modes due to TM-TE mode conversion is undesirable in traditional photonic applications since it introduces high propagation loss for TM mode and cross-talk between neighbouring components. The TE polarization is commonly used in ridge SOI waveguide to avoid this lateral leakage loss. However, the TM polarization is desirable for some application such as sensing or hybrid photonics in which strong interaction between the optical field and the material outside the waveguide core is desired. TM polarization is also required for horizontal slot waveguides to enhance the electric field in the low index material layer, and in plasmonic waveguides to achieve plasmonic modes. For these applications using TM mode, the waveguides need to be carefully designed at one of the resonant 'magic' width to minimize the leakage loss. Low leakage loss devices based on resonant 'magic' width behaviour have been demonstrated using simple ridge waveguide [29]–[32], horizontal slot waveguides [22], [33] and coupling from TM waveguide to plasmomic waveguides [34].

The results in Figs. 3 and 6 indicate that the lateral leakage loss is fairly sensitive to the waveguide width and the operating wavelength. In order to maintain the lateral leakage loss below 0.1 dB/cm, the waveguide width should be maintained within $\pm$10 nm of the 'magic' width while the wavelength should not vary more than $\pm$10 nm. To broaden the low leakage loss waveguide width and wavelength windows, waveguide structures with dimples in the center of the ridge core have been proposed [9], [10]. In this waveguide configuration, the radiating TE field consists of TE waves generated from four ridge interfaces. The phase relationship between these TE waves depends on the waveguide ridge width and the dimple width. Therefore, robust leakage cancellation can be achieved with the right combination of the waveguide width and the dimple width.

On the other hand, the strong TM-TE mode conversion and highly resonant transition from leaky to non-leaky behaviour could be useful for new photonic devices. By making deliberate use of the leakage behaviour, new photonic components can be designed. Some possible applications are discussed in the following.

A. Polarization Handling

The behaviour of high index contrast integrated photonic circuits depends strongly on the polarization state of the optical signal. Therefore, polarization handling functions are often required in circuits based on high index contrast waveguides. The strong polarization dependent leakage loss can be ultilized for polarization handling functions such as on-chip polarizers. The basic working principle of a polarizer is to have a much higher loss for one polarization compared to the other. The strong lateral leakage loss of TM polarization makes a thin-ridge SOI waveguide a perfect candidature for an on-chip TE-pass polarizer. In Ref. [35], a compact, broadband TE-pass polarizer based on a shallowly etched SOI straight waveguide was proposed and demonstrated. A 1 mm-long polarizer exhibits a high extinction ratio ($>$25 dB) over a wide wide wavelength range (100 nm).

A polarizer based on lateral leakage loss phenomenon can be very compact, insensitive to dimensional variation, broad band and insensitive to temperature variation as compared to polarizers based on other techniques such as ARROW's [36], [37], metal-cladding waveguides [38]–[40], lithium niobate waveguides [41], or liquid crystals [42]. Since this type of polarizer is a straight waveguide, it is very simple to make and readily integrated with other components in advanced silicon photonic circuits. This polarizer can be engineered to maximize the lateral leakage loss of the TM mode in order to increase the polarization extinction ratio while reducing the device length [43]. In LNOI waveguide platform, lateral leakage can occur for TM as well as TE polarizations due to strong birefringence of lithium niobate [8], [26]. Therefore, TE-pass as well as TM-pass polarizers utilizing lateral leakage on LNOI ridge waveguides can be realized [44].

B. Optical Antennas and Long Range Coupling

In integrated photonic circuits, power transferred between waveguides are often rely on evanescent coupling. This restricts

the waveguide coupling usually to nearest neighbour interactions. However, in some cases long-range coupling or by-passing nearest neighbours are also desired. In the following we highlight how lateral leakage radiation can be used for long-range coupling.

It should be noted that the lateral leakage radiation due to TM/TE conversion in thin-ridge SOI waveguides is not random radiation. Instead, the radiation is very coherent. The phase matching condition required for the conversion to occur means that the TE wave radiates at a very specific angle to the TM mode propagation axis. It is possible to manipulate the radiation angle by controlling the effective indices of the TM guided mode and/or the TE slab mode. The strength of the radiation can also be varied from zero radiation to very large radiation by waveguide geometry design [43]. These lateral leakage behaviours make a thin-ridge SOI waveguide similar to a leaky wave antenna, which is basically a waveguide structure allowing power to leak along its length [45], [46]. Similar to the application of leaky wave antennas in RF communications, the lateral leakage can be harnessed to allow optical signal transfer between well separated circuits through the unguided TE radiation. It is possible to manipulate the direction and the spatial profile of the radiated TE radiation [47], [48].

It has been shown in Section II-G that two SOI ridges can always couple to each other regardless of their separation through coupling to a common TE slab mode. This TE slab mode thus can be considered as a bus mode enabling power transfer between well separated waveguides. This provides an opportunity of performing long-range transfer between multiple waveguides without restricting the geometry to the nearest neighbour interactions. However, the unbound nature of the TE slab radiation can causes high loss and interference with other devices on the circuit. Therefore, it is desirable to suppress the power existing in this common TE slab mode while using this TE slab mode as a bus for long-range coupling. It is possible to achieve long-range coupling in thin-ridge SOI waveguides using a common TE slab bus mode without exciting this bus as well as bypassing intermediate waveguides by combining the lateral leakage behaviour and an adiabatic technique called Coherent Tunnelling Adiabatic Passage (CTAP) [49] or photonic quantum gate design [50].

V. Ridge Resonance Based on Lateral Leakage

In this Section, the diffraction behaviour of a thin-ridge SOI waveguide when it is illuminated by a broad beam of vertically confined TE slab mode from the cladding regions (as illustrated in Fig. 11) is discussed, showing that the ridge behaves like a resonator to the incident TE beam [51]. Depending on the ridge width, this resonance can also be considered as a bound state in the continuum (as described in Section III).

A. Diffraction of Wide TE Beam Incident on the Ridge

When a TE beam is incident on the ridge, one can expect that there will be some reflection due to the index difference between the cladding and ridge regions, caused by normal Fresnel reflection. It is also reasonable to expect that this TE beam can excite the TM guided mode in the ridge when they are phase-matched. The excited TM mode in the ridge can then radiate into TE beams on both sides of the ridge. Thus, the total reflected and transmitted TE field on either sides of the ridge are the superposition of TE field due to Fresnel reflection as well as leakage TE field from the excited TM mode.

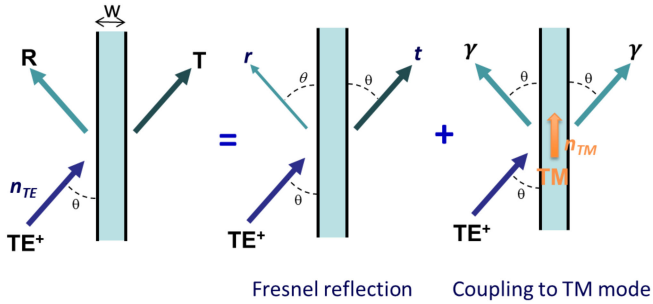

Fig. 11. TE slab obliquely incident on the ridge.

Using coupled-mode theory [52], [53], it is possible to derive a simple model to predict the behaviour of the ridge based on the propagation characteristics of the TM mode and the background Fresnel reflection and transmission coefficients. The reflection coefficient of a TE beam on the ridge can be expressed as [51]:

$$R = \frac{j\left[\left(n_{TE}^{clad}\cos\theta - N_{TM}\right)r - \gamma t\right]}{j\left(n_{TE}^{clad}\cos\theta - N_{TM}\right) + \gamma} \tag{3}$$

where γ is the imaginary part of the complex effective index of the guided TM mode, r and t are the Fresnel reflection and transmission coefficients due to the index difference at the ridge walls. Eq. 3 is equivalent to equations describing the interaction between non-resonant background process and resonant-assisted coupling process in two-port resonator systems [52], [53]. In this case, the non-resonant process is the Fresnel reflection and transmission due to the index difference at the ridge walls, while the resonant-assisted coupling is the interaction between the incident TE beam and guided TM mode. When the non-resonant process is strong, the interference between these two process can create Fano-like resonance [52] with asymmetric line shape. When the non-resonant background process due to Fresnel reflection and transmission at the ridge walls can be ignored, the reflection coefficient due to resonant-assisted process alone can be written as:

$$R = \frac{-j\gamma}{j\left(n_{TE}^{clad}\cos\theta - N_{TM}\right) + \gamma} \tag{4}$$

which has a Lorentzian line shape and is entirely determined by the propagation characteristics of the TM mode and the incident TE slab mode.

From Eq. 3, it is predicted that a strong resonance behaviour is expected when the incident TE beam is phase matched to the ridge TM mode ($n_{TE}^{clad}\cos\theta - N_{TM} = 0$). To rigorously simulate this resonant behaviour, a full-vector mode-matching model was used. Fig. 12 shows the rigorously simulated reflection as a function of the indent angle. For comparison, Fig. 12 also shows the background reflection due solely to Fresnel reflection as well as the analytically calculated reflection using Eq. 3 and Eq. 4

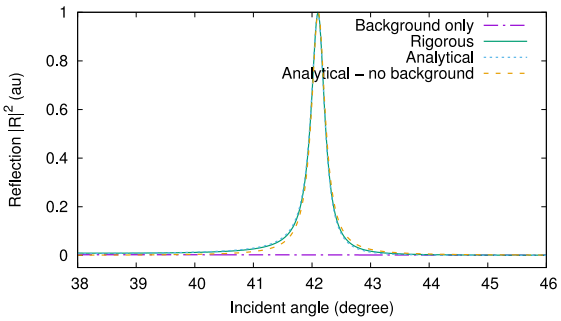

Fig. 12. Reflection as a function of incident angle, when considering only background Fresnel reflection, total reflection from rigorous mode-matching model, from analytical calculation including background reflection using Equation 3, and from analytical calculation without background reflection using Equation 4.

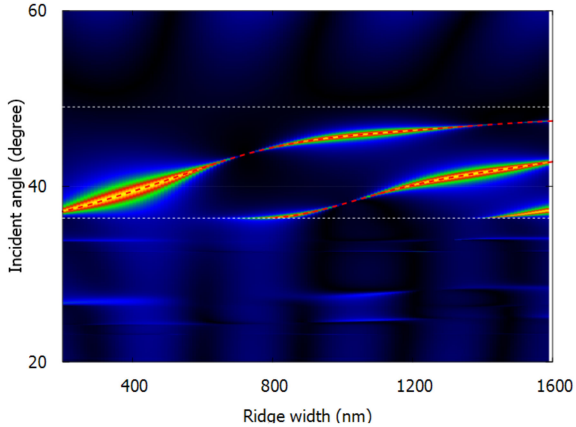

Fig. 13. Rigorously simulated reflection as a function of both ridge width and incident angle. The red dash lines are the phase-matching angles between the incident TE beam and guided TM mode.

when considering only the resonant-assisted process. Rigorous simulation reveals a strong resonant peak at the indent angle that causes phase-matching between the incident TE mode and the TM ridge mode. The analytical coupled-mode formalism, when considering both non-resonant background and resonant TE/TM coupling processes, can also predict the behaviour accurately. When ignoring the background process, the resonant behaviour close to the phase-matching condition can still be predicted very accurately by the analytical coupled-mode model with the resonant TE/TM coupling process alone.

It can be seen from Eqs. 3 and 4 that the width of the resonance depends strongly on the leakage loss of the guided TM mode in the ridge, which is a function of the ridge width. Therefore, it is expected that the ridge width has a strong impact on the resonance width. Fig. 13 shows the rigorously simulated reflection versus the incident angle and the ridge width. It is clear that when the ridge width approaches one of the 'magic' widths, the resonance width decreases. For each ridge width, the maximum reflection occurs at the incident angle resulting in phase-matching between the incident TE beam and TM guided mode. It is also noted that for large ridges, it is possible to excite multiple resonances with different angles of incident since large ridges can support multiple TM modes of different effective indices.

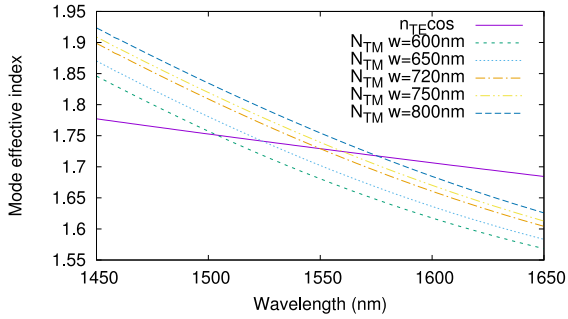

Fig. 14. Mode effective index as a function of wavelength of the incident TE slab mode and TM mode in the ridges for different ridge widths. The incident angle is fixed at an angle that results in phase-matching between incident TE slab mode and TM ridge mode for ridge width $W = 720$ nm.

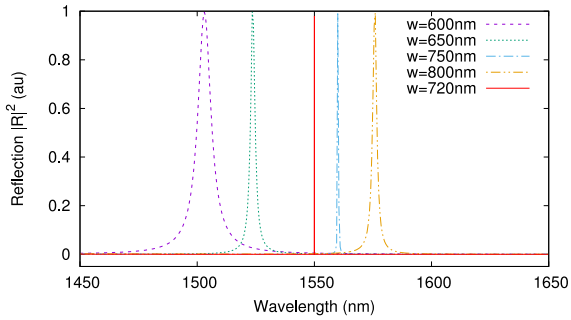

Fig. 15. Rigorously simulated reflection as a function of wavelength for different ridge widths. The incident angle was fixed.

The reflection is strongest at the phase-matching point and decreases when the phase-mismatch increases. Since the ridge TM mode and TE slab mode can have different dispersion, when the incident angle is fixed, the phase-matching condition can only occur at a specific wavelength, as illustrated in Fig. 14. Therefore, it is expected that the diffraction behaviour of incident TE beam on the ridge also depends on wavelength. Fig. 15 shows the wavelength dependence of the rigorously simulated reflection for different ridge widths when the incident angle is fixed. It is evident that the ridge acts like a resonator when illuminated with an incident TE beam. The resonant wavelengths are the wavelengths that the dispersion curves of the incident TE slab mode (n_{TE}^{clad}) and of the guided TM mode of the ridge intersect, resulting in phase-matching between the two modes. Similar to the case of varying the incident angle, the spectral line width of the resonances depends strongly on the ridge width or leakage loss of the ridge TM mode. The spectral line width is infinitely small when the ridge is close to the 'magic' width.

To further investigate the effect of ridge width on the spectral bandwidth, the Q factor of the resonance was calculated from the wavelength response for different ridge widths. For each ridge width the incident angle was adjusted so that the resonance always occurred at the wavelength of 1550 nm. Fig. 16 shows the calculated Q as a function of the ridge width. Singularities in the Q factor when the ridge width is equal to the 'magic' widths can be seen.

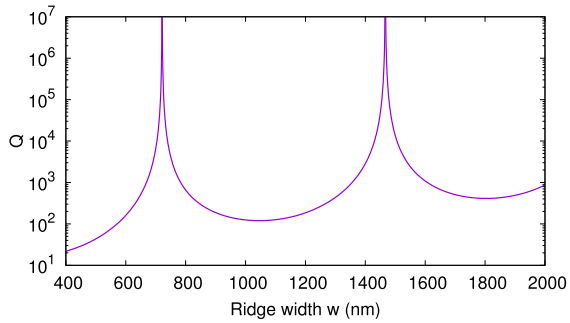

Fig. 16. Resonance quality factor Q versus the ridge width. The incident angle was adjusted so that all resonance occurred at 1550 nm wavelength.

Similar resonance behaviour has also been predicted in other waveguide platforms such as in a GaP ridge waveguide [54] or in an isolated rectangular dielectric strip above a slab waveguide [55]. However, in the later case, the resonance is not due to TE/TM coupling but due to the leakage of the guided TE mode of the isolated strip to the TE mode of the slab underneath the strip. Recently, the first experimental observation of this ridge resonance behaviour has been demonstrated [51].

B. Ridge Resonance: Opportunities and Challenges

The results in Section V-A show that unlike other types of resonators that can have cyclic spectral response, a ridge resonator has a single resonance over a broad spectral range. In addition, since a ridge resonator is based on a single ridge, its width is smaller than an optical wavelength. These unique properties allow multiple ridge resonators being coupled side by side with very small inter-cavity delay to realize tightly coupled resonator optical waveguides (CROW's) [56]. These structures can be of great interest to achieve many optical functions such as high-order filtering with flat-top pass-band, sharp roll-off and high extinction ratio which can be difficult to realize when the size of individual resonators as well as spacing between them are large. Coupled resonators using narrow resonators and with low inter-cavity delay are also a great platform to study new physical phenomena such as exceptional points or BIC's [14], [57].

It should be noted that in the investigation in Section V-A, it has been assumed that the incident TE beam is very wide, effectively considering it as an infinite planewave with single delta function angular spectral component. When the width of the incident beam is limited, it no longer can be considered as a planewave, but a superposition of planewaves propagating at different angles with a finite angular spectral distribution. The reflection and transmission of a finite width beam will depend on the width of the angular spectrum of the incident beam and the angular spectral width of the reflection. Fig. 17 shows the planewave angular spectrum of an incident Gaussian beam and the angular reflection spectrum and the corresponding electric field intensity measured at the center of the silicon layer of two ridge resonators with different widths. The incident angle was selected so that the resonators were on resonance. When the Q factor of the resonator is low, its angular spectral width is much wider than the planewave angular width of the incident beam. Hence, all planewaves that make up the incident beam are reflected with similar reflection coefficient, resulting in the reflected beam having similar intensity and spatial profile as the incident beam. However, when the resonator Q increases, the width of the anglular spectrum of its reflection profile decreases and becomes comparable to the width of the angular spectrum of the incident beam. Thus, different spectral components of the incident beam experience significantly different reflection. Therefore, the intensity of the reflection beam is much lower than that of the incident beam and the transmitted power is relatively high. In addition, the spatial profiles of the reflected and transmitted beams are different from the spatial profile of the incident field.

The above observation suggests that in order for the ridge to operate as a resonator, the angular spectral width of the incident beam must be much smaller than the angular spectral width of the ridge resonator. The higher the ridge resonator Q factor , the wider the incident beam needs to be in order to be effectively reflected. To put this finding in context, our simulations suggest that to effectively excite a ridge resonator with a Q factor of 1000, the incident beam should be wider than 1 mm and the width of the beam would scale linearliy with the resonator Q. Generating such wide beam on-chip is challenging and requires a lot of chip real estate [51], [58]. Methods to overcome this issue are currently under investigation and will be published else where.

The authors in [59] have analyzed the spatial profiles of the reflected and transmitted beams upon diffraction on a ridge at the resonant incident angle. They predict that when the angular spectrum of the incident beam is much wider than the resonant angular bandwidth of the ridge, the spatial profiles of the reflected beam and transmitted beam are the integration and differentiation of the spatial profile of the incident beam. This behaviour can also be seen from Fig. 17(d). This suggests that a simple ridge can be used as an efficient planar on-chip optical integrator as well as an differentiator.

C. Ridge Resonance as Bound-State in the Continuum

As shown in Fig. 16, the Q factor of the ridge resonance diverges to singularities when the ridge width equal to one of the 'magic' widths. This indicates the existence of BIC's [54] at these ridge widths. The bound states are non-leakage TM modes in the ridge that arise in the continuum of TE modes in the slab as discussed in Section III.

The location of these BIC's is a function of ridge geometry, wavelength and incident angle [54], but is still very robust. When one of these parameters change, a BIC does not completely disappear but moves to a different location. For a fixed operating wavelength, a 'perfect' BIC exists when the ridge width is equal to the 'magic' width of the ridge TM mode at that wavelength and the incident angle equal to the phase-matching angle. When the width of the ridge changes, the TM mode with cancelled

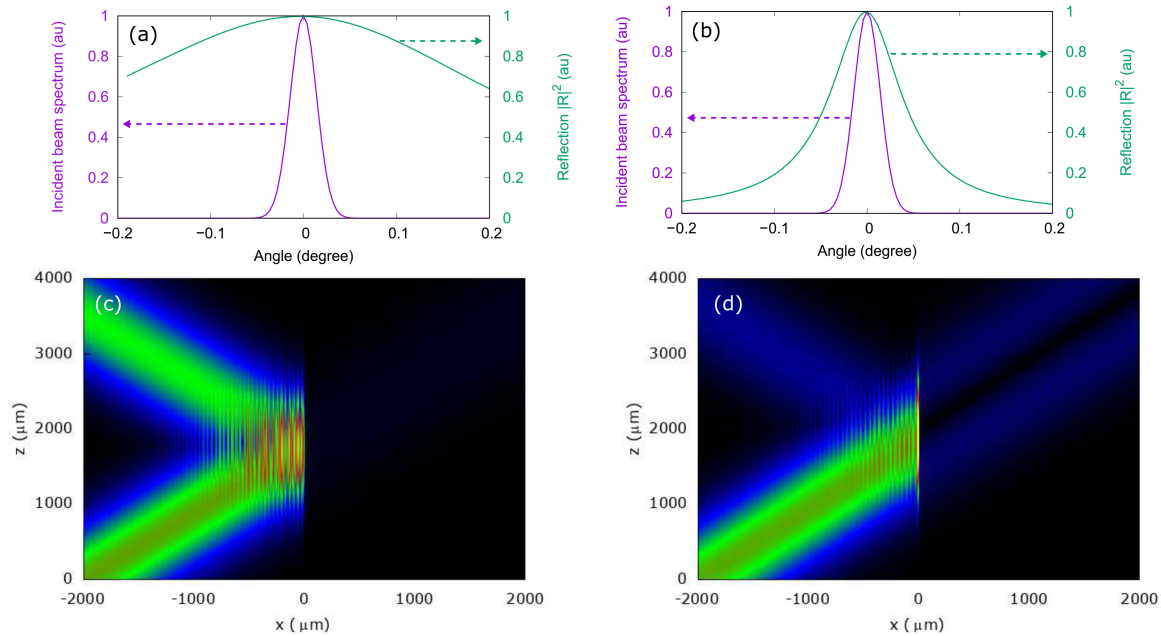

Fig. 17. Planewave spectrum of incident Gaussian beam and reflection spectrum of ridge with width (a) $W = 550$ nm and (b) $W = 650$ nm. (c) and (d) are the corresponding field intensity.

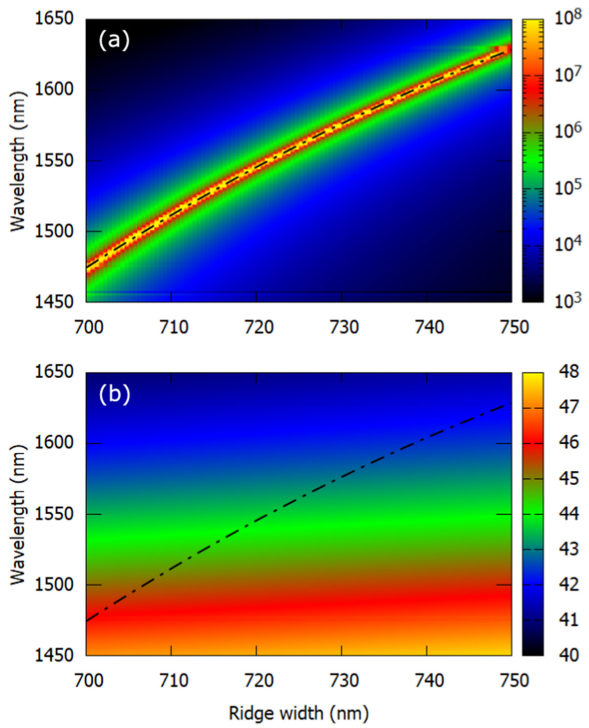

Fig. 18. (a) Ridge resonance Q as a function of both the ridge width and wavelength; and (b) corresponding phase-matching angle. The black dashed lines are the locations of BIC's.

leakage will move to a different wavelength. Therefore, the BIC will occur at different wavelength with different incident angle. Fig. 18 shows the calculated resonance Q as a function of both ridge width and wavelength when the ridge width is varied from the nominal 'magic' width at 1550 nm wavelength [Fig. 18(a)] and the corresponding phase-matching angle [Fig. 18(b)]. In Fig. 18, the locations of BIC's are indicated by the black dashed lines. As can be seen, when the ridge width changes, this BIC moves to a different wavelength and a different incident angle.

VI. Conclusion

In this paper, we have presented an overview of the lateral leakage effect in silicon photonic ridge waveguides. The origin of the leakage from guided TM mode in the ridge to coherent TE radiation into the surrounding slab have been presented. The conceptual theory as well as approaches for rigorous simulation of resonant cancellation of the lateral leakage behaviour have been given. We have also provided a detailed analysis of these behaviours in different waveguide configurations as well as discussed them in other waveguide platforms and have highlighted a number of proposed applications. We have also shown that a simple ridge can act like a resonator to a broad TE beam obliquely incident on the ridge due to the coupling between the incident TE beam and the guided TM mode supported by the ridge. The Q factor of this ridge resonance is simply determined by the width of the ridge. We have discussed how these lateral leakage, resonant leakage cancellation and ridge resonance phenomena can be treated as bound states in the continuum. The opportunities and challenges in utilizing these phenomena for new optical functions were presented. This often overlooked phenomenon can create new opportunities for polarisation manipulation, surprising coupling behaviour between well separated waveguides and emerging opportunities for wavelength filtering. By drawing parallels with the physics of bound states in the continuum there are opportunities to open new frontiers for silicon photonics as a platform to investigate

fundamental physics. By looking back and finding analogies with radio frequency devices we may find new opportunities for photonic wavelength filters and even optical antennas for free space transmission based on lateral leakage.

REFERENCES

[1] S.-T. Peng and A. A. Oliner, "Leakage and resonance effects on strip waveguides for integrated optics," *IEICE Trans.*, vol. 61, no. 3, pp. 151–153, 1978.

[2] S.-T. Peng and A. A. Oliner, "Guidance and leakage properties of a class of open dielectric waveguides: Part I–mathematical formulations," *IEEE Trans. Microw. Theory Techn.*, vol. MTT-29, no. 9, pp. 843–855, Sep. 1981.

[3] M. Webster, R. Pafchek, A. Mitchell, and T. Koch, "Width dependence of inherent TM-mode lateral leakage loss in silicon-on-insulator ridge waveguides," *IEEE Photon. Technol. Lett.*, vol. 19, no. 6, pp. 429–431, Mar. 2007.

[4] A. A. Oliner, S.-T. Peng, T.-I. Hsu, and A. Sanchez, "Guidance and leakage properties of a class of open dielectric waveguides: Part II–new physical effects," *IEEE Trans. Microw. Theory Techn.*, vol. MTT-29, no. 9, pp. 855–869, Sep. 1981.

[5] K. Ogusu, "Optical strip waveguide-A detailed analysis including leaky modes," *J. Opt. Soc. Amer.*, vol. 73, pp. 353–357, 1983.

[6] P. Muellner, N. Finger, and R. Hainberger, "Lateral leakage in symmetric SOI rib-type slot waveguides," *Opt. Express*, vol. 16, no. 1, pp. 287–294, 2008.

[7] X. Xu, S. Chen, J. Yu, and X. Tu, "An investigation of the mode characteristics of SOI submicron rib waveguides using the film mode matching method," *J. Opt. A, Pure Appl. Opt.*, vol. 11, no. 1, pp. 015508–015514, 2009.

[8] E. Saitoh, Y. Kawaguchi, K. Saitoh, and M. Koshiba, "A design method of lithium niobate on insulator ridge waveguides without leakage loss," *Opt. Express*, vol. 19, no. 17, pp. 15 833–15 842, 2011.

[9] M. Koshiba, K. Kakihara, and K. Saitoh, "Reduced lateral leakage losses of TM-like modes in silicon-on-insulator ridge waveguides," *Opt. Lett.*, vol. 33, no. 17, pp. 2008–2010, 2008.

[10] K. Kakihara, K. Saitoh, and M. Koshiba, "Generalized simple theory for estimating lateral leakage loss behavior in silicon-on-insulator ridge waveguides," *J. Lightw. Technol.*, vol. 27, no. 23, pp. 5492–5499, Dec. 1, 2009.

[11] B. A. Dorin and W. N. Ye, "Conditions for single-mode and birefringence-free ultrasmall SOI rib waveguides at 1310 nm," *J. Lightw. Technol.*, vol. 31, no. 21, pp. 3420–3424, Nov. 2013.

[12] F. T. Dullo, J. Tinguely, S. A. Solbø, and O. G. Hellesø, "Single-mode limit and bending losses for shallow rib $Si_3 N_4$ waveguides," *IEEE Photon. J.*, vol. 7, no. 1, Feb. 2015, Art. no. 2700511.

[13] C.-L. Zou *et al.*, "Guiding light through optical bound states in the continuum for ultrahigh-Q microresonators," *Laser Photon. Rev.*, vol. 9, no. 1, pp. 114–119, 2015.

[14] C. W. Hsu, B. Zhen, A. D. Stone, J. D. Joannopoulos, and M. Soljačić, "Bound states in the continuum," *Nature Rev. Mater.*, vol. 1, 2016, Art. no. 16048.

[15] T. G. Nguyen, R. S. Tummidi, T. L. Koch, and A. Mitchell, "Rigorous modeling of lateral leakage loss in SOI thin-ridge waveguides and couplers," *IEEE Photon. Technol. Lett.*, vol. 21, no. 7, pp. 486–488, Apr. 2009.

[16] A. S. Sudbo, "Improved formulation of the film mode matching method for mode field calculations in dielectric waveguides," *Pure Appl. Opt.*, vol. 3, pp. 381–388, May 1994.

[17] K. Ogusu, S. Kawakami, and S. Nishida, "Optical strip waveguide: An analysis," *Appl. Opt.*, vol. 18, no. 6, pp. 908–914, 1979.

[18] K. Ogusu and I. Tanaka, "Optical strip waveguide: An experiment," *Appl. Opt.*, vol. 19, no. 19, pp. 3322–3325, Oct. 1980.

[19] A. P. Hope, T. G. Nguyen, A. Mitchell, and W. Bogaerts, "Quantitative analysis of TM lateral leakage in foundry fabricated silicon rib waveguides," *IEEE Photon. Technol. Lett.*, vol. 28, no. 4, pp. 493–496, Feb. 2016.

[20] T. Ako, J. Beeckman, W. Bogaerts, and K. Neyts, "Tuning the lateral leakage loss of TM-like modes in shallow-etched waveguides using liquid crystals," *Appl. Opt.*, vol. 53, no. 2, pp. 214–220, Jan. 2014.

[21] T. Ako *et al.*, "Electrically tuneable lateral leakage loss in liquid crystal clad shallow-etched silicon waveguides," *Opt. Express*, vol. 23, no. 3, pp. 2846–2856, Feb. 2015.

[22] R. M. Pafchek, J. Li, R. S. Tummidi, and T. L. Koch, "Low loss Si–SiO_2-Si 8-nm slot waveguides," *IEEE Photon. Technol. Lett.*, vol. 21, no. 6, pp. 353–355, Mar. 2009.

[23] Q. Lu, W. Guo, D. C. Byrne, and J. F. Donegan, "Compact 2-D FDTD method combined with Padé approximation transform for leaky mode analysis," *J. Lightw. Technol.*, vol. 28, no. 11, pp. 1638–1645, Jun. 2010.

[24] Y.-D. Yang, Y.-Z. Huang, W.-H. Guo, Q. Lu, and J. F. Donegan, "Enhancement of quality factor for TE whispering-gallery modes in microcylinder resonators," *Opt. Express*, vol. 18, no. 12, pp. 13 057–13 062, Jun. 2010.

[25] Y.-D. Yang and Y.-Z. Huang, "Investigation of vertical leakage loss for whispering-gallery modes in microcylinder resonators," *J. Lightw. Technol.*, vol. 29, no. 18, pp. 2754–2760, Sep. 2011.

[26] A. Boes *et al.*, "Improved second harmonic performance in periodically poled LNOI waveguides through engineering of lateral leakage," *Opt. Express*, vol. 27, no. 17, pp. 23 919–23 928, Aug. 2019.

[27] T. G. Nguyen, R. S. Tummidi, T. L. Koch, and A. Mitchell, "Lateral leakage in TM-like whispering gallery mode of thin-ridge silicon-on-insulator disk resonators," *Opt. Lett.*, vol. 34, no. 7, pp. 980–982, 2009.

[28] L. Prkna, M. Hubálek, and J. Ctyroký, "Field modeling of circular microresonators by film mode matching," *IEEE J. Sel. Topics Quantum Electron.*, vol. 11, no. 1, pp. 217–223, Jan./Feb. 2005.

[29] R. Pafchek *et al.*, "Low-loss silicon-on-insulator shallow-ridge TE and TM waveguides formed using thermal oxidation," *Appl. Opt.*, vol. 48, no. 5, pp. 958–963, 2009.

[30] M. M. Milošević *et al.*, "A thermal and low loss ridge silicon waveguides," in *Proc. SPIE*, vol. 7606, 2010, Art. no. 76061A.

[31] G. Reed *et al.*, "The UK silicon photonics project," in *Proc. SPIE*, vol. 7719, 2010, Art. no. 77190A.

[32] R. M. Briggs, I. M. Pryce, and H. A. Atwater, "Compact silicon photonic waveguide modulator based on the vanadium dioxide metal-insulator phase transition," *Opt. Express*, vol. 18, no. 11, pp. 11 192–11 201, May 2010.

[33] R. M. Briggs, M. Shearn, A. Scherer, and H. A. Atwater, "Wafer-bonded single-crystal silicon slot waveguides and ring resonators," *Appl. Phys. Lett.*, vol. 94, 2009, Art. no. 021106.

[34] R. M. Briggs, J. Grandidier, S. P. Burgos, E. Feigenbaum, and H. A. Atwater, "Efficient coupling between dielectric-loaded plasmonic and silicon photonic waveguides," *Nano Lett.*, vol. 10, no. 12, pp. 4851–4857, 2010.

[35] D. Dai, Z. Wang, N. Julian, and J. E. Bowers, "Compact broadband polarizer based on shallowly-etched silicon-on-insulator ridge optical waveguides," *Opt. Express*, vol. 18, no. 26, pp. 27 404–27 415, Dec. 2010.

[36] Y. Kokubun and S. Asakawa, "Arrow-type polarizer utilizing form birefringence in multilayer first cladding," *IEEE Photon. Technol. Lett.*, vol. 5, no. 12, pp. 1418–1420, Dec. 1993.

[37] J. Y. Lin and A. K. Chu, "Arrow-type polarizer with large core diameter and high extinction ratio," *IEEE Photon. Technol. Lett.*, vol. 16, no. 10, pp. 2278–2280, Oct. 2004.

[38] G. Li and A. Xu, "Analysis of the TE-pass or TM-pass metal-clad polarizer with a resonant buffer layer," *J. Lightw. Technol.*, vol. 26, no. 10, pp. 1234–1241, May 2008.

[39] X. Sun, M. Z. Alam, S. J. Wagner, J. S. Aitchison, and M. Mojahedi, "Experimental demonstration of a hybrid plasmonic transverse electric pass polarizer for a silicon-on-insulator platform," *Opt. Lett.*, vol. 37, no. 23, pp. 4814–4816, Dec. 2012.

[40] M. Z. Alam, J. S. Aitchison, and M. Mojahedi, "Compact and silicon-on-insulator-compatible hybrid plasmonic TE-pass polarizer," *Opt. Lett.*, vol. 37, no. 1, pp. 55–57, Jan. 2012.

[41] R.-C. Twu, C.-C. Huang, and W.-S. Wang, "TE-pass Zn-diffused $LiNbO_3$ waveguide polarizer," *Microw. Opt. Technol. Lett.*, vol. 48, no. 11, pp. 2312–2314, 2006.

[42] A. d'Alessandro, B. Bellini, D. Donisi, R. Beccherelli, and R. Asquini, "Nematic liquid crystal optical channel waveguides on silicon," *IEEE J. Quantum Electron.*, vol. 42, no. 10, pp. 1084–1090, Oct. 2006.

[43] R. S. Tummidi, T. G. Nguyen, A. Mitchell, and T. L. Koch, "An ultra-compact waveguide polarizer based on "anti-magic widths"," in *Proc. 8th IEEE Int. Conf. Group IV Photon.*, Sep. 2011, pp. 104–106.

[44] E. Saitoh, Y. Kawaguchi, K. Saitoh, and M. Koshiba, "TE/TM-pass polarizer based on lithium niobate on insulator ridge waveguide," *IEEE Photon. J.*, vol. 5, no. 2, 2013, Art. no. 6600610.

[45] D. Lioubtchenko, S. Tretyakov, and S. Dudorov, *Millimeter-Wave Waveguides*, vol. 114. New York, NY, USA: Springer, 2003.

[46] A. Oliner and D. Jackson, *Leaky-Wave Antennas*, 4th ed. New York, NY, USA: McGraw Hill, 2007.

[47] N. Dalvand, T. G. Nguyen, R. S. Tummidi, T. L. Koch, and A. Mitchell, "Thin-ridge silicon-on-insulator waveguides with directional control of lateral leakage radiation," *Opt. Express*, vol. 19, no. 6, pp. 5635–5643, Mar. 2011.
[48] N. Dalvand, T. G. Nguyen, T. L. Koch, and A. Mitchell, "Thin shallow-ridge silicon-on-insulator waveguide transitions and tapers," *IEEE Photon. Technol. Lett.*, vol. 25, no. 2, pp. 163–166, Jan. 2013.
[49] A. P. Hope, T. G. Nguyen, A. D. Greentree, and A. Mitchell, "Long-range coupling of silicon photonic waveguides using lateral leakage and adiabatic passage," *Opt. Express*, vol. 21, no. 19, pp. 22 705–22 716, Sep. 2013.
[50] A. P. Hope, T. G. Nguyen, A. Mitchell, and A. D. Greentree, "Adiabatic two-photon quantum gate operations using a long-range photonic bus," *J. Phys. B, Atomic, Mol. Opt. Phys.*, vol. 48, no. 5, Feb. 2015, Art. no. 055503.
[51] T. G. Nguyen *et al.*, "Ridge resonance in silicon photonics harnessing bound states in the continuum," *Laser Photon. Rev.*, to be published, doi: 10.1002/lpor.201900035.
[52] K. X. Wang, Z. Yu, S. Sandhu, and S. Fan, "Fundamental bounds on decay rates in asymmetric single-mode optical resonators," *Opt. Lett.*, vol. 38, no. 2, pp. 100–102, Jan. 2013.
[53] S. Fan, W. Suh, and J. D. Joannopoulos, "Temporal coupled-mode theory for the fano resonance in optical resonators," *J. Opt. Soc. Am. A*, vol. 20, no. 3, pp. 569–572, Mar. 2003.
[54] E. A. Bezus, D. A. Bykov, and L. L. Doskolovich, "Bound states in the continuum and high-Q resonances supported by a dielectric ridge on a slab waveguide," *Photon. Res.*, vol. 6, no. 11, pp. 1084–1093, Nov. 2018.
[55] M. Hammer, L. Ebers, and J. Förstner, "Oblique evanescent excitation of a dielectric strip: A model resonator with an open optical cavity of unlimited Q," *Opt. Express*, vol. 27, no. 7, pp. 9313–9320, Apr. 2019.
[56] A. Yariv, Y. Xu, R. K. Lee, and A. Scherer, "Coupled-resonator optical waveguide:A proposal and analysis," *Opt. Lett.*, vol. 24, no. 11, pp. 711–713, Jun. 1999.
[57] M. Y. Nada, M. A. K. Othman, and F. Capolino, "Theory of coupled resonator optical waveguides exhibiting high-order exceptional points of degeneracy," *Phys. Rev. B*, vol. 96, Nov. 2017, Art. no. 184304.
[58] G. Ren, T. G. Nguyen, and A. Mitchell, "Gaussian beams on a silicon-on-insulator chip using integrated optical lenses," *IEEE Photon. Technol. Lett.*, vol. 26, no. 14, pp. 1438–1441, Jul. 2014.
[59] E. A. Bezus, L. L. Doskolovich, D. A. Bykov, and V. A. Soifer, "Spatial integration and differentiation of optical beams in a slab waveguide by a dielectric ridge supporting high-Q resonances," *Opt. Express*, vol. 26, no. 19, pp. 25 156–25 165, Sep. 2018.

Thach G. Nguyen received the B.Eng. degree (Hons.) and the Ph.D. degree from RMIT University, Melbourne, VIC, Australia, in 1998 and 2006, respectively. From 1999 to 2002, he was an R&D Engineer with VITECO - VNPT Vietnam. He is currently a Senior Lecturer with the School of Engineering, RMIT University. His current research interests include integrated optics, silicon photonics devices and circuits, integrated photonic design methods, numerical methods for integrated photonics, and microwave photonics.

Andreas Boes received the B.Eng. and M.Eng. degrees in electrical engineering from the University of Applied Sciences Karlsruhe, Karlsruhe, Germany, in 2012, and the Ph.D. degree in electrical engineering from RMIT University, Melbourne, VIC, Australia, in 2016. From 2017 to 2018, he was a Visiting Postdoctoral Research Fellow with the University of California, Santa Barbara. He is currently a Postdoctoral Research Fellow with the School of Engineering, RMIT University and a team leader with the Integrated Photonics and Applications Centre (InPAC). His research interests include microtechnology, integrated optical circuits, nonlinear optics, optoelectronics, and optical communications.

Arnan Mitchell (SM'19) was born in Dublin, Ireland, in 1973. He received the B.Tech (Hons) degree from Macquarie University, North Ryde, NSW, Australia, in 1993, and the Ph.D. degree from RMIT University, Melbourne, VIC, Australia, in 2000. He is a Distinguished Professor with the School of Engineering, RMIT University and the Director of the RMIT Micro Nano Research Facility and the Integrated Photonics and Applications Centre. He is a highly multidisciplinary researcher working in microchip technologies combining light, sound, fluids, and electronics with applications spanning radar systems for defence, high-speed fibre optic communications, and point of care diagnostic systems for biomedicine. He is committed to translating technology from the research laboratory into the hands of end users and has dedicated much of his career to building diverse teams and comprehensive micro and nanotechnology infrastructure to enable breakthrough discoveries to achieve real-world impact.